NANO · MICRO small

Supporting Information

for *Small*, DOI 10.1002/smll.202308369

Reaction with Water Vapor Defines Surface Reconstruction and Membranolytic Activity of Quartz Milled in Different Molecular Environments

*Chiara Bellomo, Valeria Lagostina, Cristina Pavan, Maria Cristina Paganini and Francesco Turci**

Reaction with Water Vapor Defines Surface Reconstruction and Membranolytic Activity of Quartz Milled in Different Molecular Environments

Chiara Bellomo[ab], Valeria Lagostina[a], Cristina Pavan[abc], Maria Cristina Paganini[ad], Francesco Turci[ab*].

[a]Department of Chemistry, University of Turin, Italy

[b]"G. Scansetti" Interdepartmental Centre for Studies on Asbestos and Other Toxic Particulates, University of Turin, Italy

[c]Louvain Centre for Toxicology and Applied Pharmacology, Université catholique de Louvain, Belgium

[d]NIS interdepartmental Centre for Nanomaterials for Industry and Sustainability , University of Turin, Italy

*Corresponding author

Abstract: Industrial processing of quartz (SiO_2) and quartz-containing materials produce toxic dusts. Fracturing quartz crystals opens the Si–O bond and produces highly reactive surface species which mainly react with molecules like water and oxygen. This surface-reconstruction process forms silanols (Si–OH) on the quartz surface, which can damage biological membranes under specific configurations. To comprehend the impact of the quartz surface restructuring on membranolytic activity, we evaluated the formation and reactivity of quartz radicals produced in four distinct molecular environments with EPR spectroscopy and we measured their membranolytic activity through *in vitro* hemolysis test. The four molecular environments were formulated with and without molecular water vapor and oxygen ($\pm H_2O/\pm O_2$). The absence of water favored the formation of surface radical species. In water-rich environments, diamagnetic species prevailed due to radical recombination. Quartz milled in $-H_2O/\pm O_2$ acquired membranolytic activity when exposed to water vapor, unlike quartz milled in $+H_2O/\pm O_2$. After being stabilized by reaction with water vapor, the membranolytic activity of quartz was maintained over time. It was demonstrated that the type and the reactivity of radical sites on quartz were modulated by outer molecular environment, ultimately determining the biological activity of milled quartz dust.

Table of Contents

S1. Preliminary Milling of Quartz Crystals and microstructural analysis of mineral quartz milled in different molecular environments.

The first comminution step was performed in an agate jar in open air following a procedure reported in the literature.[1] High purity mineral quartz characterized by centimetric crystals, (Figure S1 A) was subjected to a preliminary milling step to obtain a fine powder with a negligible specific surface area (PM quartz SSA = 0.3 m^2/g). The EPR spectrum of PM quartz from 100 to 4000 G indicates the absence of any detectable radical species, as well as the absence of paramagnetic metal species derived from Fe, Al and Mn. Around 1.5 g of PM quartz was milled down to a respirable size following a procedure reported in the Experimental Section that was performed in four different environmental conditions (−H_2O/−O_2, −H_2O/+O_2, +H_2O/−O_2,+H_2O/+O_2). The Specific Surface Area (SSA, Figure S1 B) was evaluated by measuring Kr physisorption at −196 °C and applying the Brunauer, Emmett, and Teller (BET) method. The ASAP 2020 apparatus (Micromeritics, Norcross, USA) was used. Before analysis, samples were outgassed at 150 °C for 2 h to remove physiosorbed molecules. Figure S1 C reports about micrographs of the milled quartz obtained in the four environments. The particle morphology was assessed by (SEM). The analyses were performed with a FIB-FESEM/EBSD/TOF-SIMS Tescan S9000G, using a secondary electron detector with an accelerating voltage of 15-5 keV.

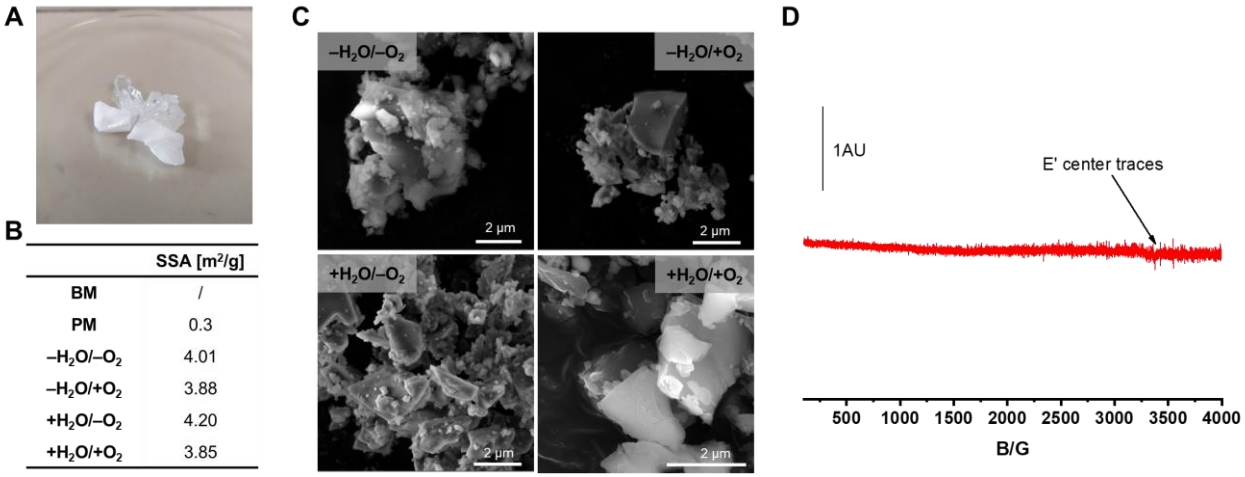

	SSA [m^2/g]
BM	/
PM	0.3
–H_2O/–O_2	4.01
–H_2O/+O_2	3.88
+H_2O/–O_2	4.20
+H_2O/+O_2	3.85

Figure S1: Principal physicochemical characteristics of mineral quartz before and after milling. A) Image of centimetric quartz crystals before milling. B) Specific surface area (SSA) of the samples before milling (BM), after the pre milling (PM) and after the second milling step for each environmental condition. C) SEM micrographs of quartz samples milled in different environmental conditions. D) EPR spectrum of PM quartz. Spectrum recorded between 100 and 4000 G at 77K. The other parameters are reported in the experimental procedures.

To investigate whether the four different molecular environments produced samples with similar morphology/size and microstructural properties, an analysis of the particle size distribution was performed with automated image analysis (FPIA) and microstructural X-ray Powder Diffraction (XRD) was carried out with samples in powder form. Particle size distribution was assessed using a flow particle image analyser (FPIA-3000S; Malvern Instruments) by injecting 5 mL of the particle suspension through a flat cell where images of the particles are captured using stroboscopic illumination and a charge-coupled device camera. Particle suspensions of 1 mg/mL in water were previously sonicated for 2 min in an ultrasonic bath before injection. Data were processed by the Sysmex FPIA software (version 00-13). The detection range was 0.8 to 100 µm. Crystallinity of the four samples and size of the crystallites was evaluated by using a Panalytical X-pert Pro MPD (Cu Kα1 = 1.54059 Å, Kα2 = 1.54446 Å) in Bragg-Brentano geometry. Patterns were collected in the 2θ range (from 10 to 120°), with a time step of 30 s. The Rietveld refinement [2] of the measured diffraction patterns has been performed using Materials Analysis Using Diffraction (MAUD) software.[3] The instrumental function was determined using LaB_6 NIST standard (660b). Data in Figure S1bis and Table S1 illustrate that crystal morphology and crystalline microstructure are largely preserved throughout the four different milling environments. Specifically, the particle size distribution and circularity shape factor are virtually superimposable for the four milled samples (see. Fig. S1bis A and Tab. S1, CE diameters). Identical cell parameters are obtained by Rietveld refinement of the measured diffraction pattern and the slight difference in crystallite average size, from 353 to 461 nm, might result from the different electrostatic adhesion forces observed for quartz milled in the absence or presence of water vapor (−H_2O; +H_2O).

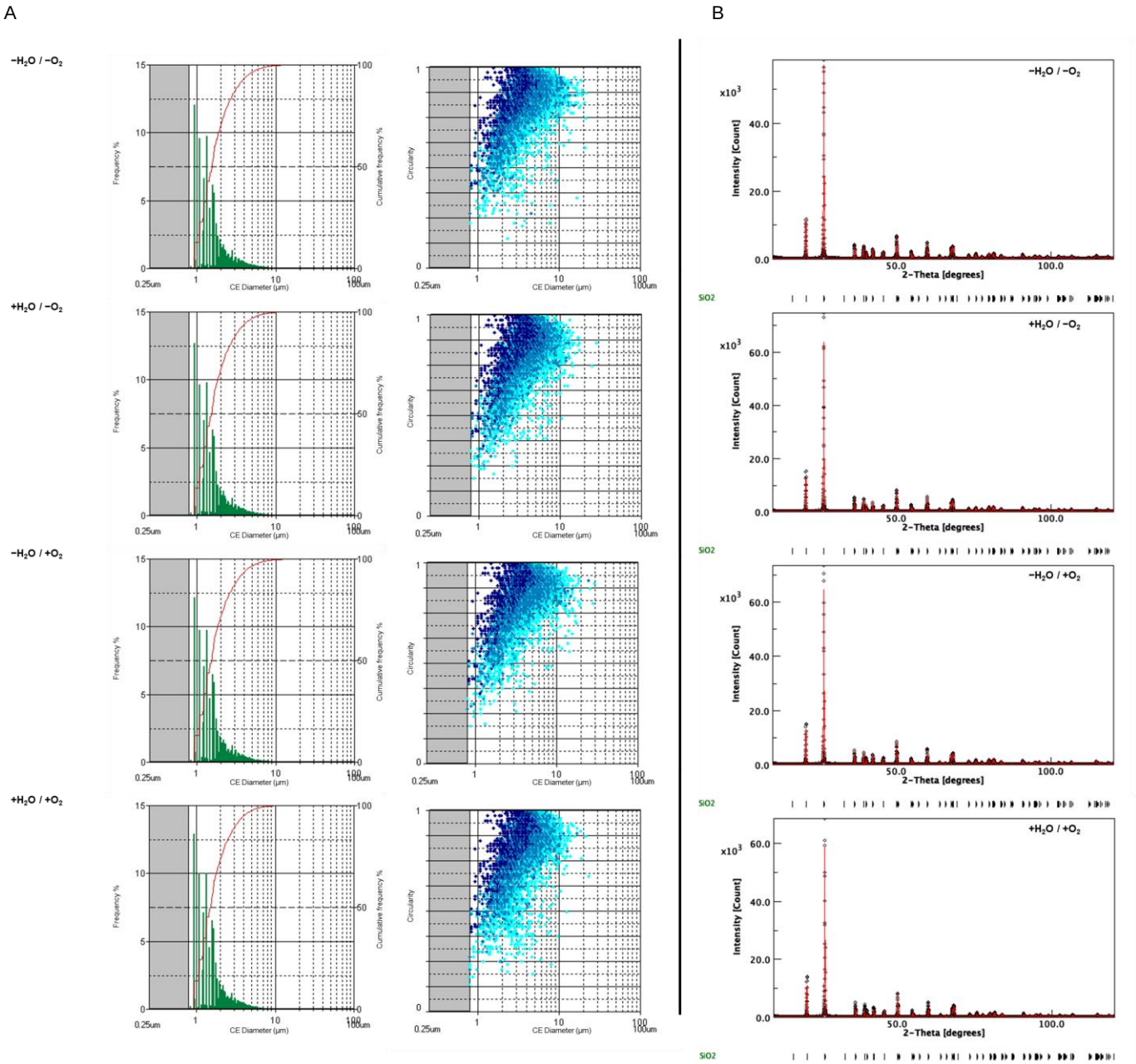

Figure S1bis: Microstructural characterization of the quartz samples milled in different environments. A) Particle size distribution and 2D-scatter plot of the circularity shape parameter vs. CE particle diameter of the four samples, assessed though FPIA analysis. B) X-ray diffractograms of the four samples are largely superimposable. No other crystalline phases were detected during the analysis.

Table S1: Dimensional and microstructural analysis of the quartz samples milled in the four different environments. The average particle diameter expressed as circle equivalent (CE) diameter and the value of the CE diameter below which 90%, 50% and 10% of observations fall (D90, D50 and D10) were reported.

	CE diameter (µm) frequency quantiles			**Cell parameters and crystallite size ± standard error**		
	10%	**50%**	**90%**	**a (Å)**	**c (Å)**	**Crystallite size (nm)**
$-H_2O / -O_2$	0.94	1.6	3.4	4.914	5.407	353 ± 5
$+H_2O / -O_2$	0.94	1.6	3.3	4.914	5.407	461 ± 3
$-H_2O / +O_2$	0.94	1.6	3.4	4.914	5.407	379 ± 3
$+H_2O / +O_2$	0.94	1.5	3.2	4.914	5.407	407 ± 7

S2. Study of the attenuation frequencies/MW power to optimize EPR signal.

Peroxyl radicals and surface-bound superoxide radicals have an opposite trend than silyl radicals. At higher attenuation frequencies the silyl radical is dominant (38dB, equivalent to 0.03 mW). At lower attenuation frequencies, peroxyl and superoxide radicals are predominant (18dB = 3 mW). The 28dB attenuation (0.3 mW) was selected and used to record all the EPR spectra in the manuscript, because all the species were clearly visible.

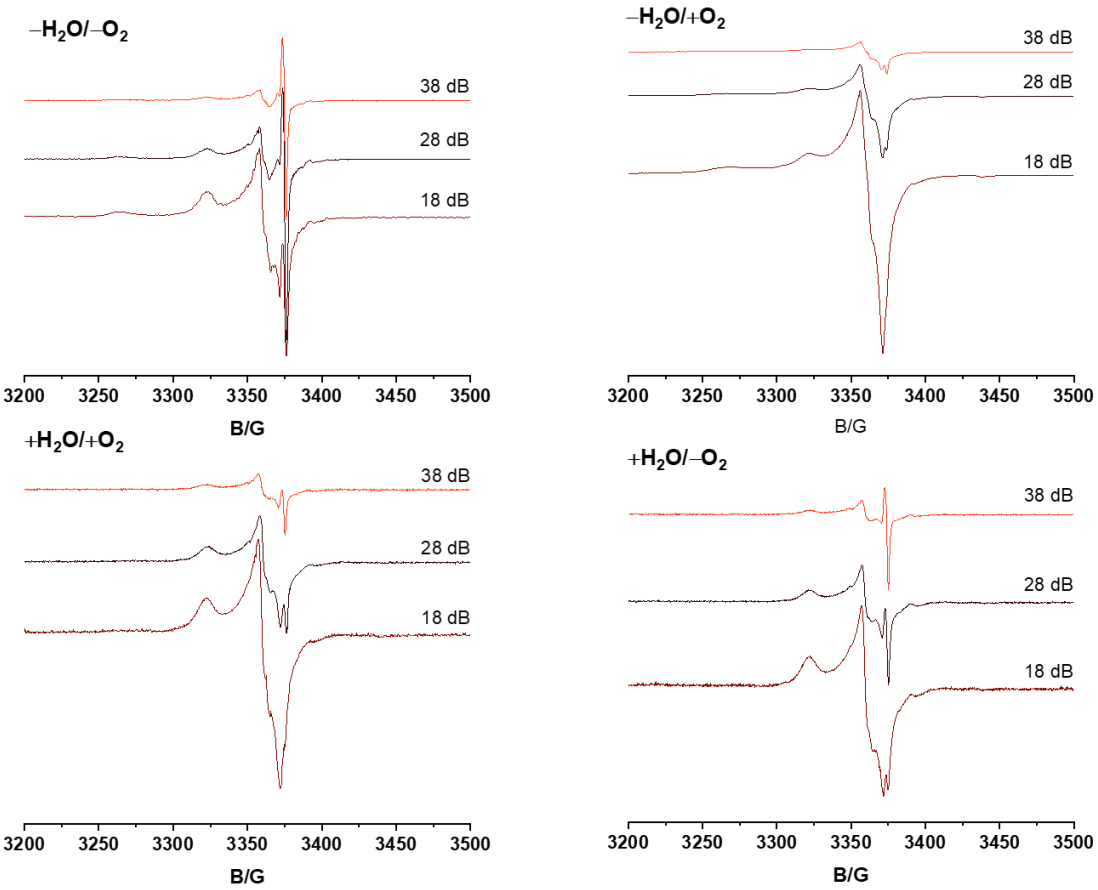

Figure S2: EPR spectra of the four milled quartzes at different attenuation frequencies.

S3. Simulation of EPR spectra and deconvolution of every species.

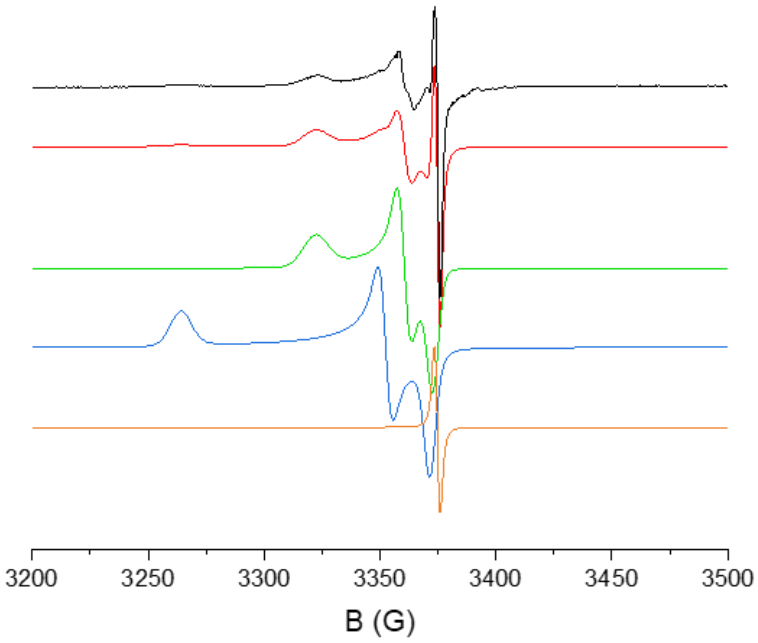

Figure S3A: Experimental (black) and simulated (red) X-band CW-EPR spectrum of quartz milled in $-H_2O/-O_2$ environment. The deconvolution of the simulated spectrum is reported as follow: $Si^{\bullet}$ (orange), $SiOO^{\bullet}$ (blue), and $Si^{+}O_2^{-\bullet}$ (green).

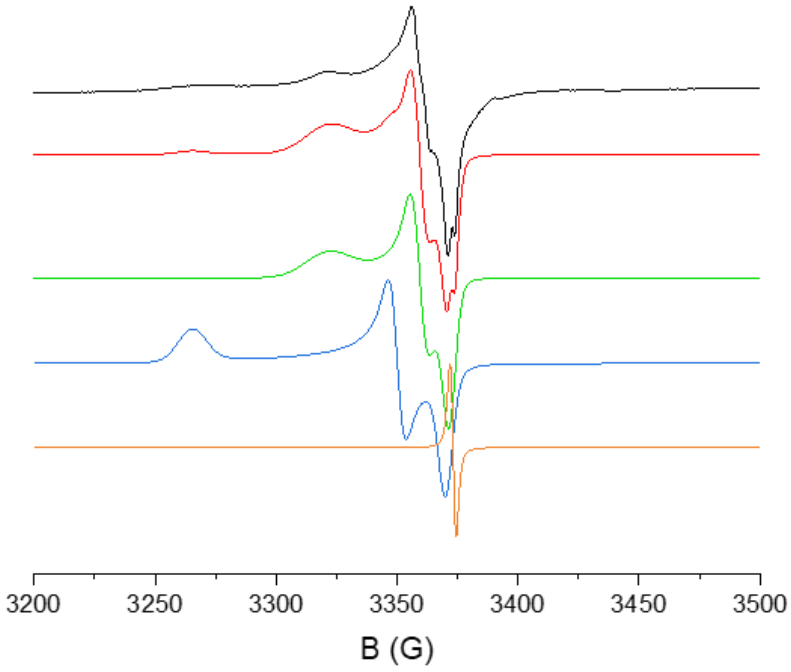

Figure S3B: Experimental (black) and simulated (red) X-band CW-EPR spectrum of quartz milled in $-H_2O/+O_2$ environment. The deconvolution of the simulated spectrum is reported as follow: $Si^{\bullet}$ (orange), $SiOO^{\bullet}$ (blue), and $Si^{+}O_2^{-\bullet}$ (green).

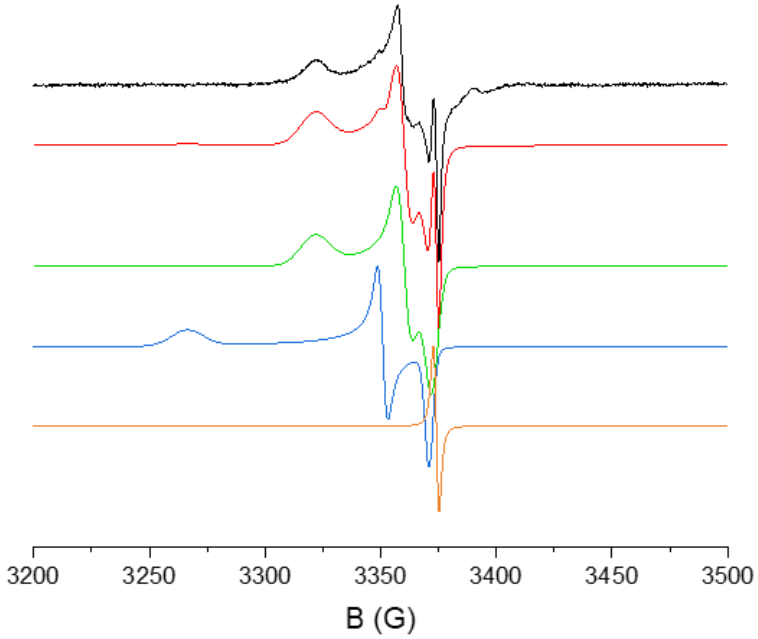

Figure S3C: Experimental (black) and simulated (red) X-band CW-EPR spectrum of quartz milled in $+H_2O/-O_2$ environment. The deconvolution of the simulated spectrum is reported as follow: $Si^{\bullet}$ (orange), $SiOO^{\bullet}$ (blue), and $Si^{+}O_2^{-\bullet}$ (green).

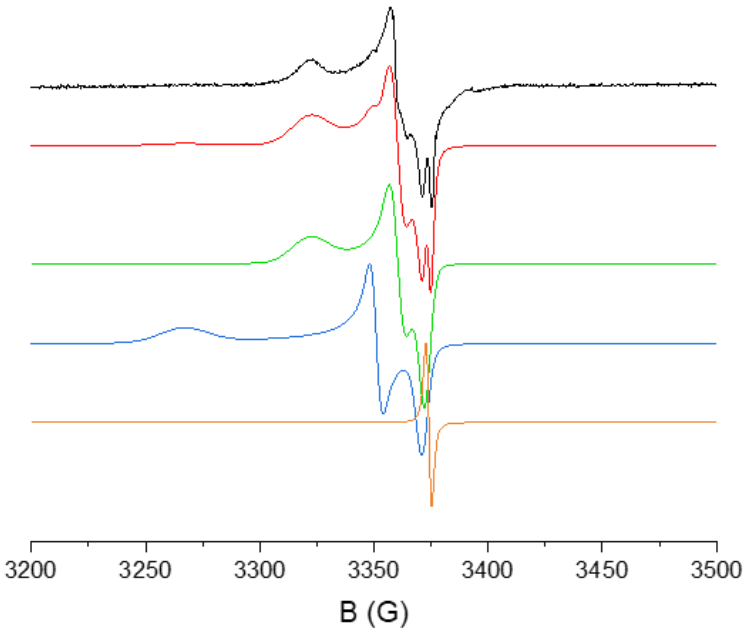

Figure S3D: Experimental (black) and simulated (red) X-band CW-EPR spectrum of quartz milled in $+H_2O/+O_2$ environment. The deconvolution of the simulated spectrum is reported as follow: $Si^{\bullet}$ (orange), $SiOO^{\bullet}$ (blue), and $Si^{+}O_2^{-\bullet}$ (green).

S4. Occurrence of surface-bound superoxide radical

Surface bound superoxide radical ($Si^+ O_2^{-\bullet}$) is supposed to form by the reduction of molecular oxygen from an electron donor centre. In water- and oxygen-free environment ($–H_2O/–O_2$), traces of molecular oxygen might still be present in the milling environment and be located either in the milling apparatus (jar porosity) or occur interstitially the quartz crystals. In this case, the extremely low presence of O_2 renders O_2 the limiting reagent for the reduction that yields superoxide. To prove this hypothesis, quartz was ball milled in the same environment for a longer time (350 rpm, 5 hours). In Figure S4 are reported the two $–H_2O/–O_2$ quartzes milled in different condition. To better visualize the differences, the sample milled at 250 rpm was multiplied by 5.5.

The quartz milled for 5 hours showed a much lower relative intensity of the signal associated to the surface-bound superoxide radical with respect to E' and $SiO^{\bullet}$. The magnified inset (A') further highlights the different intensity and proves that silyl and peroxyl radicals amount increase proportionally to the milling time and energy, while the surface-bound superoxide radical, the amount of which is limited to the scarce presence of molecular oxygen present in the milling environment.

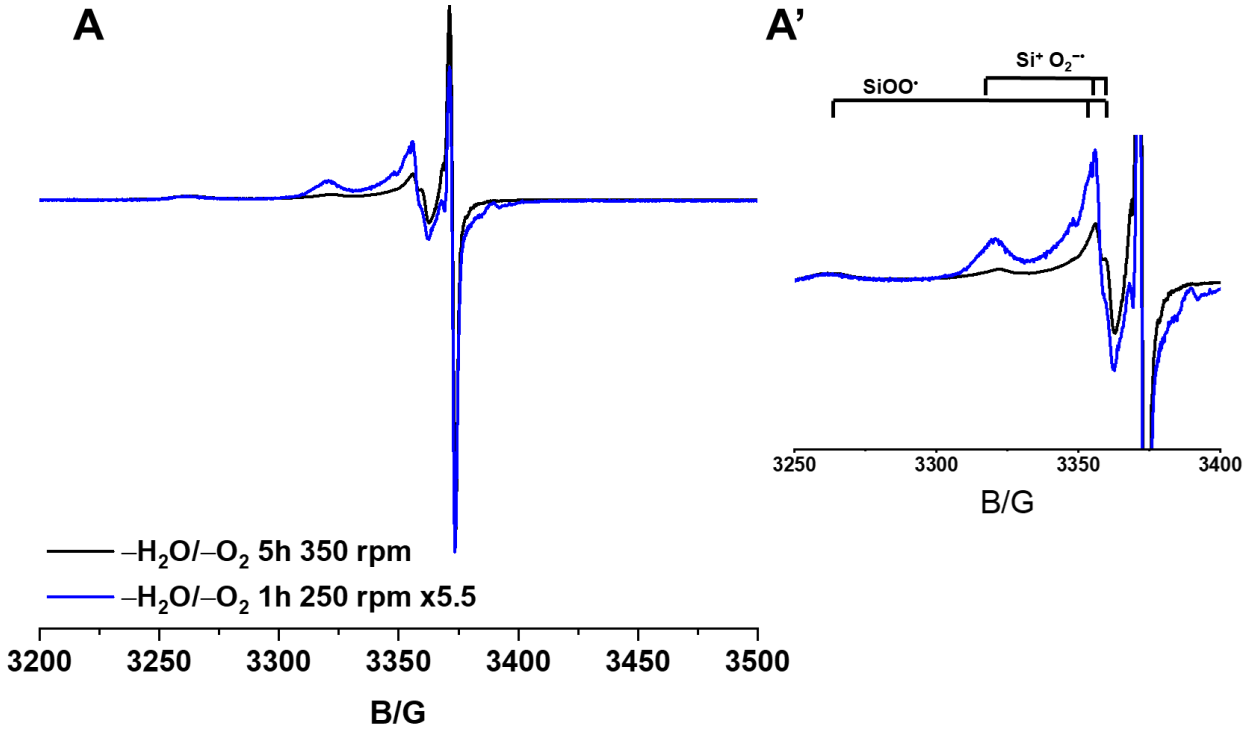

Figure S4: EPR spectra (at 77K) of quartz milled in $–H_2O/–O_2$ environment at two different milling times (1 h and 5 h). The $–H_2O/–O_2$ 1h at 250 rpm intensity is multiplied by 5.5 to help a direct comparison of the two spectra. Full spectra (A) and detail of the surface-bound superoxide radical and the peroxyl radical components (A').

S5. Ageing / stability of radicals with time.

–H_2O/–O_2 quartz after milling was kept in a glove box after milling. After 30 days, quartz was sealed in an EPR cell inside the glove box and its EPR spectra was acquired. The spectrum kept in an inert environment, without water vapor, maintain the 70% of the total amount of radicals, according to the double integrated values.

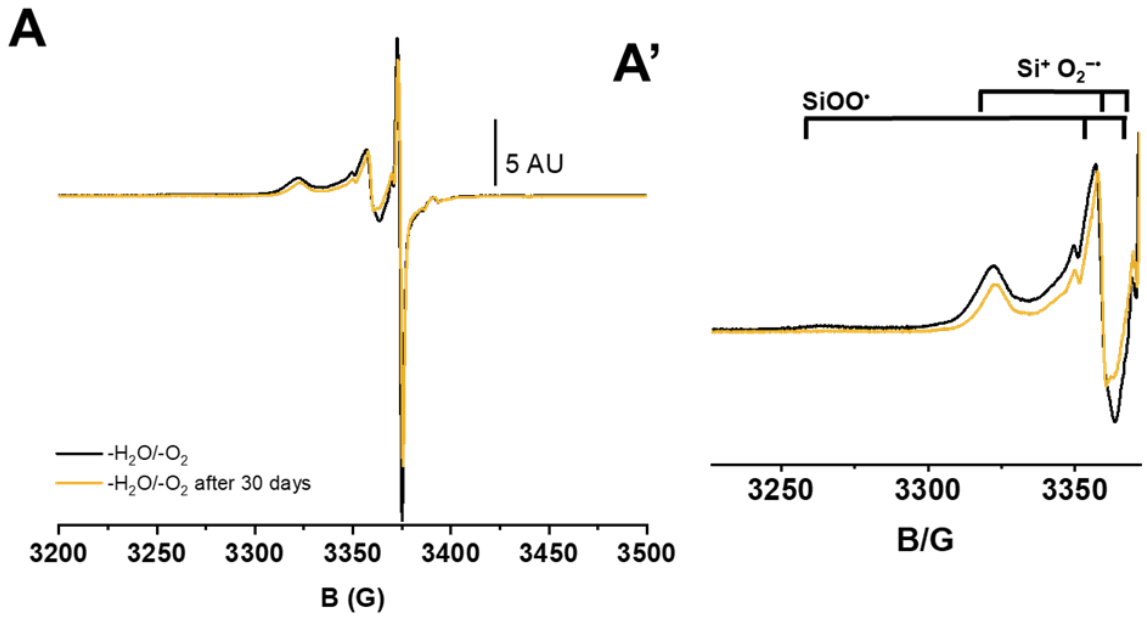

Figure S5: –H_2O/–O_2 EPR spectra immediately after milling (back line) and after 30 days of milling. A' is the magnification of 3200-3400 G section of the spectra.

S6. Reaction of surface radicals with molecular probes (O_2 and CO)

The $–H_2O/–O_2$ quartz was charged in the EPR cell in glove box. The EPR cell was sealed, pumped in vacuum line and gas was expanded in the vacuum line. The cell was then sealed and analyzed through EPR.

i. Oxygen gas (purity 5.5) was contacted with quartz in vacuum line in the same fashion as water vapor, both at RT and 77K, without further purifications (Figure S6A)

ii. CO (purity 99%) was contacted with quartz with the same experimental setup, without further purifications (Figure S6B).

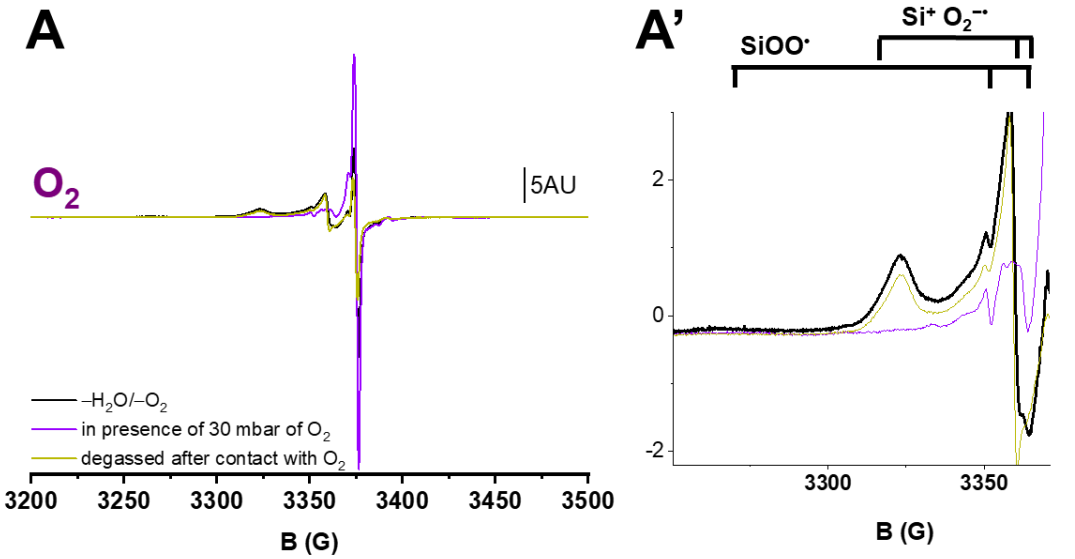

Figure S6A: $–H_2O/–O_2$ exposed to molecular oxygen. (A) $–H_2O/–O_2$ in presence of molecular oxygen at 77K and subsequent degassing (at 77K). (A') detail of the peroxide/superoxide signal before and after exposure to molecular oxygen.

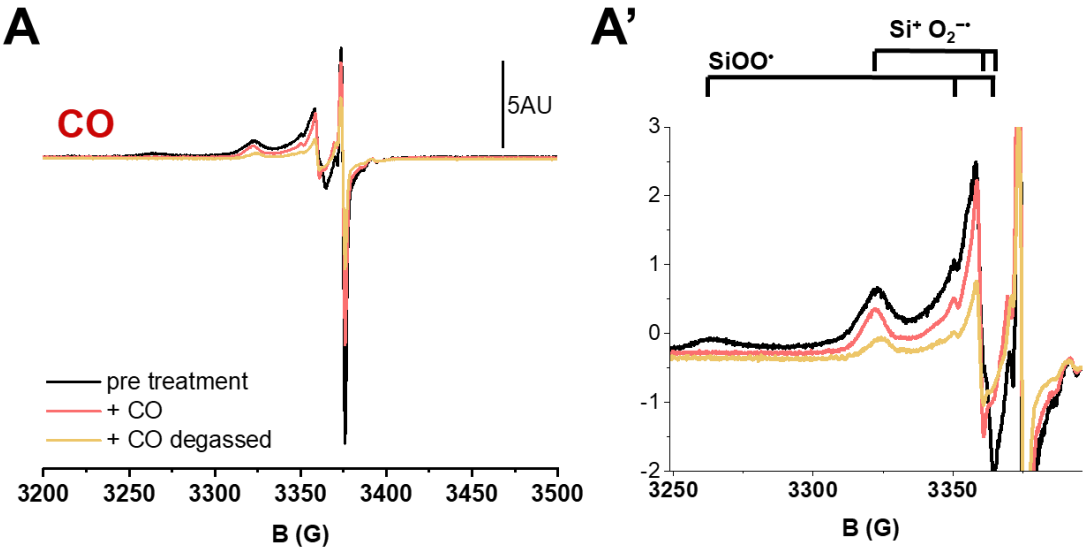

Figure S6B: Treatment of $–H_2O/–O_2$ with CO. (A) full spectrum, and (A') magnification of the 3250-3400 region to highlight the selective suppression of the peroxyl radical. Spectra were recorded at 77K.

S7. Thermal annealing of quartz radicals

Quartz was sealed inside an EPR cell and degassed in a vacuum line. Thermal treatments were performed on the same sample consecutively for 45 minutes in dynamic vacuum and after every treatment a spectrum was collected. The analysis was performed after degassing to avoid effects of O_2 in the EPR analysis. The treatments were performed consecutively at rising temperatures on the same sample.

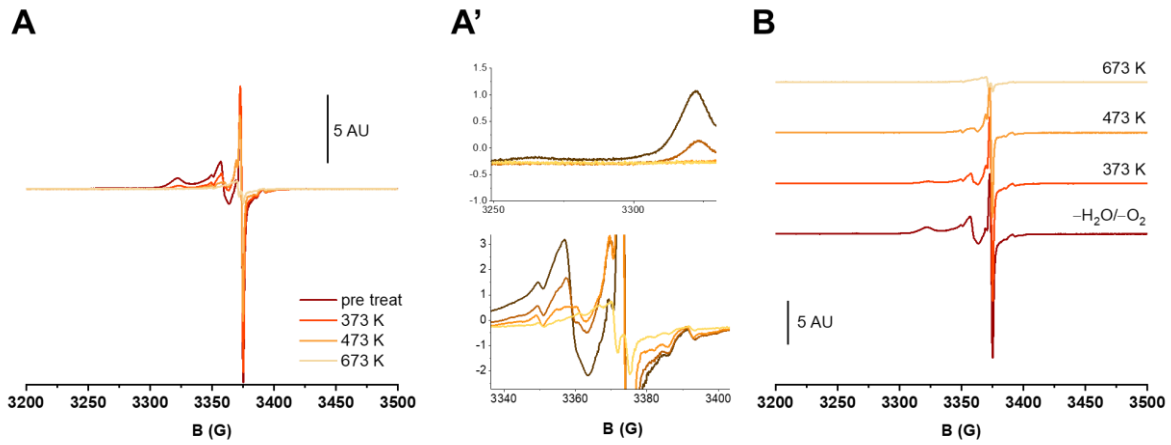

Figure S7: $–H_2O/–O_2$ subjected to thermal treatments. Dynamic vacuum thermal treatment at 373, 473, 673 K for t = 45 min each, on the same sample Full spectra (A), inset of the 3340-3400 B range (A'), and stacked spectra (B).

Author Contributions

Chiara Bellomo, Ph.D. (Conceptualization: Equal; Investigation: Lead; Methodology: Lead; Visualization: Lead; Writing – original draft: Equal; Writing – review & editing: Equal)
Valeria Lagostina (Formal analysis: Supporting; Investigation: Supporting; Methodology: Supporting; Visualization: Supporting; Writing – original draft: Supporting)
Cristina Pavan (Conceptualization: Equal; Formal analysis: Supporting; Funding acquisition: Lead; Methodology: Equal; Supervision: Equal; Writing – original draft: Supporting; Writing – review & editing: Supporting)
Maria Cristina Paganini (Conceptualization: Supporting; Methodology: Supporting; Supervision: Equal; Writing – original draft: Supporting; Writing – review & editing: Supporting)
Francesco Turci (Conceptualization: Lead; Funding acquisition: Lead; Methodology: Lead; Supervision: Lead; Writing – original draft: Equal; Writing – review & editing: Lead)

References

[1] C. Pavan, R. Santalucia, R. Leinardi, M. Fabbiani, Y. Yakoub, F. Uwambayinema, P. Ugliengo, M. Tomatis, G. Martra, F. Turci, D. Lison, B. Fubini, *Proceedings of the National Academy of Sciences* **2020**, *117*, 27836-27846.
[2] R. Young, *New York* **1993**.
[3] L. Lutterotti, *Nuclear Instruments and Methods in Physics Research Section B: Beam Interactions with Materials and Atoms* **2010**, *268*, 334-340.